Constrained Object Tracking on Compact One-dimensional Manifolds Based on Directional Statistics

Gerhard Kurz, **Florian Faion**, and **Uwe D. Hanebeck**
Intelligent Sensor-Actuator-Systems Laboratory (ISAS)
Institute for Anthropomatics
Karlsruhe Institute of Technology (KIT), Germany
gerhard.kurz@kit.edu, florian.faion@kit.edu, uwe.hanebeck@ieee.org

***Abstract*—In this paper, we present a novel approach for tracking objects whose movement is constrained to a compact one-dimensional manifold, for example a conveyer belt or a mobile robot whose movement is restricted to tracks. Standard approaches either ignore the constraint at first and retroactively move the estimate to lie on the manifold, or consider the tracking problem on a manifold but falsely assume a Gaussian distribution. Our method explicitly takes the actual topology into account from the beginning and relies on special types of probability distributions defined on the proper manifold. In particular, we consider objects moving along a closed one-dimensional track, for example an ellipse, a polygon, or similar closed shapes. This shape is transformed to a circle with a homeomorphism. Thus, we can apply a recursive circular filtering algorithm to the constrained tracking problem. Finally, the estimate is transformed back to the original manifold. We evaluate the proposed method in an experiment by tracking a toy train moving along a track and comparing the results to those of traditional approaches for this problem.**

***Index Terms*—circular estimation, manifold, wrapped normal distribution, homeomorphism, periodic**

I. Introduction

Tracked objects can sometimes be subject to certain constraints enforced by physical properties of the considered setup. In this paper, we consider objects whose movement is restricted to a one-dimensional manifold. Intuitively, the objects are only able to move along a one-dimensional line which extends through two- or three-dimensional space in a possibly curved and complicated fashion. In particular, we consider the case where this line actually forms a closed loop, so an object traveling in one direction along the line will, at some point, return to its original position. In order to track the object, we desire to estimate its position by recursively combining noisy measurements received from a suitable sensor in order to obtain an estimate of the object's current location.

Constrained object tracking can be found in various applications. Typical examples of objects moving along a one-dimensional manifold include conveyer belts as they might be found in industrial settings, robots moving along rails, or even roller coasters. For the purpose of this paper, we consider the example of a toy train moving along a track as depicted in Fig. 1.

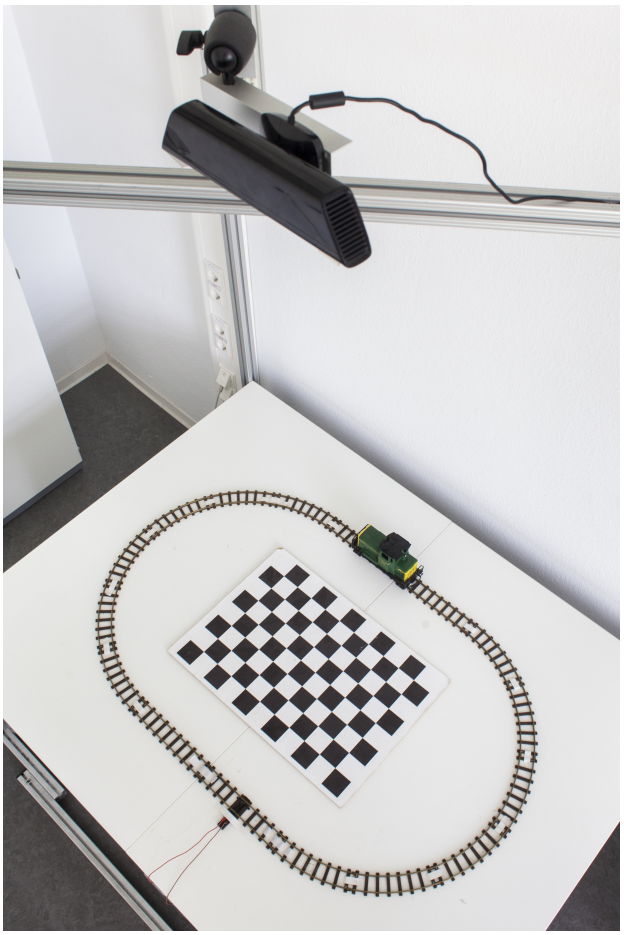

Fig. 1: Considered scenario: A toy train moves along a periodic track and is observed by a Microsoft Kinect from a bird's eye view.

The key idea of our approach is the use of a so called length-ratio-preserving homeomorphism, which maps the original manifold to a manifold for which a filtering algorithms is known. This map preserves the topological structure and the ratio between the length of any two injective smooth curves.

Consequently, we can use this map to transform the estimation problem to a different manifold and apply circular filtering algorithms to certain one-dimensional manifolds.

Directional statistics is a branch of statistics that considers directional quantities rather than real-valued quantities. In particular, directional statistics can be used to describe periodic phenomena such as angles or points on a circle. Classical results in directional and circular statistics can be found in the well-known book by Mardia and Jupp [1] as well as Jammalamadaka and Sengupta's work [2].

Directional filtering algorithms can be derived from results in directional statistics. A circular filter based on the von Mises distribution has been proposed in [3] and [4]. In previous work, we have introduced a circular filter based on the wrapped normal, von Mises, and wrapped Dirac mixture distributions [5], which we apply in this paper. There are some other examples of directional filters, for example based on projected Gaussians [6], [7] or the Bingham distribution [8].

The advantage of directional filters compared to traditional approaches based on the Gaussian distribution consists in the correct handling of periodicity. In particular in situations where the uncertainty is large, ignoring periodicity can lead to low estimation quality. Directional filters, however, can handle large uncertainties properly and produce superior results [3], [5].

The main contribution of this paper is the application of a circular filter in the area of constrained object tracking. Unlike previous approaches, not only do we take the constraint into account, we also handle the circular nature of the considered problem correctly. In particular, we provide a clean derivation of the topological transformation that is required to reduce the original problem to a circular estimation problem.

This paper is structured as follows. First, we introduce some of the standard approaches to tackle the problem of constrained object tracking in Sec. II. Then, we define the required topological transformation in Sec. III and explain the circular filtering algorithm in Sec. IV. Finally, we present experimental results comparing the proposed method to standard approaches in Sec. V and form a conclusion in Sec. VI.

II. State of the Art

Incorporating state constraints into algorithms for Bayesian object tracking is a well-studied field of research. A comprehensive overview of methods for linear and non-linear constraints is given in [9], [10]. Roughly speaking, these approaches can be divided into several classes:

1) Performing estimation in the original unconstrained state space
   a) employing pseudo-measurements that constantly pull the state towards the constraints [11].
   b) using a post-processing correction in or after the measurement update to force the state to fulfill the constraints [12], [13].
   c) modifying the system model and its uncertainty characteristics [14].
2) Performing estimation in the constrained state space by defining a suitable state representation, similar to the approach taken in this work.

All strategies have their advantages and disadvantages. However, defining an appropriate state representation is the only way that truly respects the fact that the object's movement is constrained from the beginning, whereas the other approaches initially violate the constraint and try to retroactively enforce it. For this reason, we favor the approach to perform estimation in the constrained state space.

Before we introduce the details of the proposed approach for constrained object tracking, we outline standard approaches that are commonly used. These will serve as a basis for comparison in the experiments in Sec. V.

A. 1D Kalman Filter

The first standard approach we consider is the application of a standard one-dimensional Kalman filter [15] after reducing the considered scenario to a one-dimensional problem. For this purpose, a similar transform as described in Sec. III can be used. However, the Kalman filter operates on the real axis, which is not homeomorphic to the periodic train track. Thus, the transformation does not preserve the true topology of the original problem. Consequently, the transformation is not continuous. As we will show in the evaluation, tracking fails when this discontinuity is reached.

B. 2D Kalman Filter

A second standard approach is the use of a two-dimensional Kalman filter. This may seem natural for a two-dimensional tracking problem, but the constraint can be violated by both the prediction and the update steps of the Kalman filter. In order to enforce the constraint, we project the current estimate to the closest point on the track after each update step, similar to [13]. It should be noted that the uncertainty is represented by a two-dimensional covariance ellipse even though the true uncertainty is only one-dimensional as it solely extends along the track.

III. Constrained Object Tracking by Topological Transformation

In the following, we only consider constraints that restrict the movement of the tracked object to a one-dimensional manifold. Some examples of one-dimensional manifolds are depicted in Fig. 2. First, we discuss the topological motivation for transforming a one-dimensional manifold to a circle. Subsequently, we will perform the required transformation for the example of a train track, which we will later use in our experiments.

A. Topological Motivation

An n-dimensional *manifold* is a topological space that locally behaves like $\mathbb{R}^n$. In this paper, we only consider one-dimensional manifolds, i.e., manifolds that locally behave like $\mathbb{R}$. Furthermore, we assume that the tracked object moves in either $\mathbb{R}^2$ or $\mathbb{R}^3$, so we restrict ourselves to manifolds that are subsets of $\mathbb{R}^2$ or $\mathbb{R}^3$.

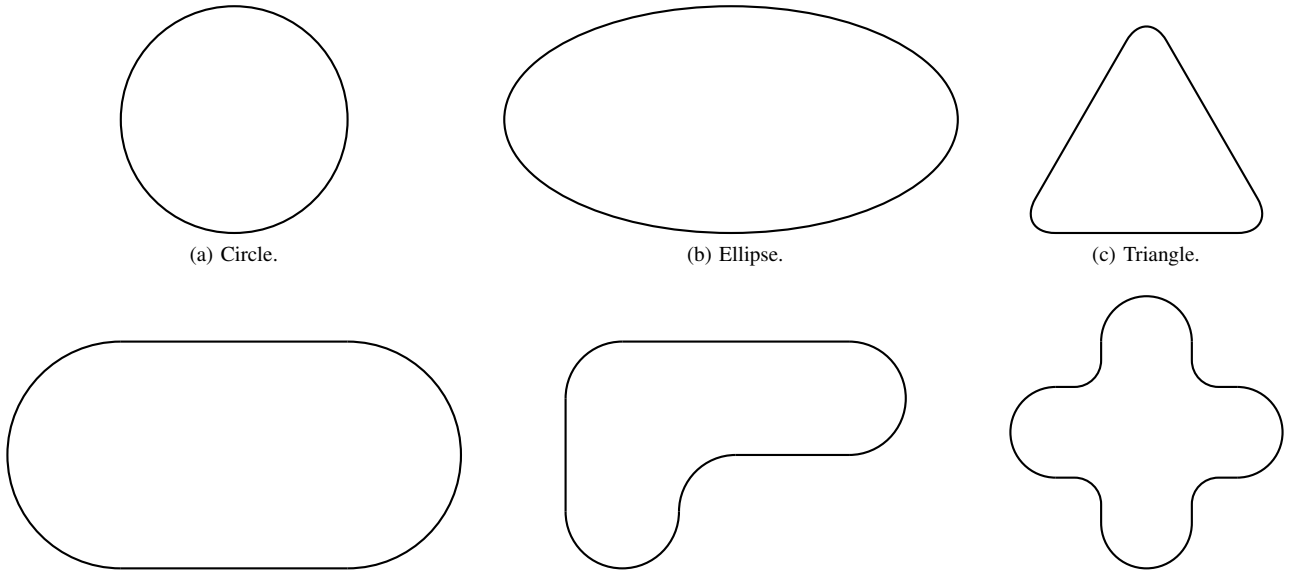

(a) Circle. (b) Ellipse. (c) Triangle.

(d) Track. (e) L-shape. (f) Plus-shape.

Fig. 2: Examples of one-dimensional manifolds. Please note that the interior area is not part of the manifold.

In order to create maps between different manifolds (or more general, topological spaces), we introduce the notion of a homeomorphism.

Definition 1. *(Homeomorphism)*

A map $f : X \to Y$ between topological spaces X and Y is called a homeomorphism *if f is bijective and both f and f^{-1} are continuous.*

According to this definition, a homeomorphism is a structure-preserving map between topological spaces. Two topological spaces X and Y are said to be *homeomorphic*, i.e., topologically indistinguishable, if a homeomorphism between them exists.

Since we are not only interested in topological properties but also in geometric properties of the manifold, we need to define a *metric* on one-dimensional manifolds. Since we only consider manifolds that are subsets of $\mathbb{R}^2$ or $\mathbb{R}^3$, we use the metric induced by the Euclidean metric on the superset $\mathbb{R}^2$ or $\mathbb{R}^3$. The distance between two points on the manifold is thus given by the length of the geodesic, i.e., the shortest curve between them measured according to the Euclidean metric in $\mathbb{R}^2$ or $\mathbb{R}^3$. The length of an injective smooth curve $\alpha : [0, 1] \to \mathbb{R}^2$ or $\alpha : [0, 1] \to \mathbb{R}^3$ is given by

$$||\alpha|| := \int_0^1 ||\alpha'(t)|| \, \mathrm{d}t \ ,$$

where $||\cdot||$ is the Euclidean metric.

In order to transform probability distributions between different manifolds, we need to put a restriction on the types of homeomorphisms we can use. Ideally, a homeomorphism should preserve the length of any injective smooth curve on the manifold.

Definition 2. *(Length-preserving homeomorphism)*

We call a homeomorphism $f : X \to Y$ length-preserving *if for all injective smooth curves $\alpha : [0, 1] \to X$, we have*

$$||\alpha|| = ||f(\alpha)|| \ .$$

If length is preserved, it is trivial to transform a probability distribution defined on one manifold X to a probability distribution defined on the other manifold Y.

However, we would like to apply a circular filter that is based on probability distributions on the unit circle S^1. Since the manifold representing the constraint does not have length 2π in general, we have to weaken our definition to allow uniform scaling to a manifold of different length.

Definition 3. *(Length-ratio-preserving homeomorphism)*

We call a homeomorphism $f : X \to Y$ length-ratio-preserving *if for all injective smooth curves $\alpha : [0, 1] \to X$*

$$||\alpha|| = c \cdot ||f(\alpha)||$$

for a fixed scaling factor $c > 0$.

A length-ratio-preserving homeomorphism does not require the two manifolds to be of equal length, but still allows a trivial transformation of the probability distribution to a different manifold. It follows from the definition that the length-ratio of two curves remains the same after transformation, i.e., for all injective smooth curves $\alpha_1, \alpha_2 : [0, 1] \to X$

$$||\alpha_2|| > 0 \Rightarrow ||f(\alpha_2)|| > 0 \text{ and } \frac{||\alpha_1||}{||\alpha_2||} = \frac{||f(\alpha_1)||}{||f(\alpha_2)||} \ .$$

Obviously, any length-preserving homeomorphism is length-ratio-preserving for $c = 1$.

Theorem 1. *Let $f : X \to Y$ be a length-ratio-preserving homeomorphism between one-dimensional manifolds and p_Y :*

$Y \to \mathbb{R}_{\geq 0}$ *a probability density on* Y*. Then* $p_X : X \to \mathbb{R}_{\geq 0}$ *with* $x \mapsto c \cdot p_Y(f(x))$ *and* $c = \frac{||X||}{||Y||}$ *is a probability density on* X *and for all injective smooth curves* $\alpha : [0,1] \to X$ *it holds that the probabilities fulfill the equation*

$$\mathbb{P}(a \in \alpha([0,1])) = \mathbb{P}(f(a) \in f(\alpha([0,1]))) \ .$$

Proof. By applying the substitution rule twice, we obtain

$$\begin{aligned}
\mathbb{P}(a \in \alpha([0,1])) &= \int_{a \in \alpha([0,1])} p_X(a) \ \mathrm{d}a \\
&= \int_0^1 p_X(b) \cdot ||\alpha'(b)|| \ \mathrm{d}b \\
&= \int_0^1 c \cdot p_Y(f(b)) \cdot ||\alpha'(b)|| \ \mathrm{d}b \\
&= \int_0^1 p_Y(b) \cdot ||f(\alpha'(b))|| \ \mathrm{d}b \\
&= \int_{f(a) \in \alpha([0,1])} p_Y(f(a)) \ \mathrm{d}f(a) \\
&= \mathbb{P}(f(a) \in f(\alpha([0,1]))) \ .
\end{aligned}$$

□

Examples of original and transformed probability density functions are depicted in Fig. 4.

B. One-Dimensional Train Track

We consider the track $T \subseteq \mathbb{R}^2$ as depicted in Fig. 3. It consists of four segments, two half circles and two straight lines. The track can be parameterized by two quantities, the radius $r > 0$ and the line length $d > 0$. The total length of the track is thus $l = 2\pi r + 2d$. The set $T = T_1 \cup T_2 \cup T_3 \cup T_4$ is given by

$$\begin{aligned}
T_1 &= \{(r\cos(\phi), r\sin(\phi))^T \mid \phi \in (\pi/2, 3\pi/2]\} \ , \\
T_2 &= \{(x, r)^T \mid x \in [0, d)\} \ , \\
T_3 &= \{(r\cos(\phi) + d, r\sin(\phi))^T \mid \phi \in (-\pi/2, \pi/2]\} \ , \\
T_4 &= \{(x, -r)^T \mid x \in (0, d]\} \ .
\end{aligned}$$

We parameterize the circle S^1 as the half-open interval $[0, 2\pi)$ and define the map

$$f : S^1 \cong [0, 2\pi) \to T$$

from the unit circle to the track according to

$$f(\alpha) = \begin{cases} f_1(\alpha \cdot \frac{l}{2\pi}) \ , & 0 \leq \alpha < \frac{2\pi}{l} r\pi \\ f_2(\alpha \cdot \frac{l}{2\pi}) \ , & \frac{2\pi}{l} r\pi \leq \alpha < \frac{2\pi}{l}(r\pi + d) \\ f_3(\alpha \cdot \frac{l}{2\pi}) \ , & \frac{2\pi}{l}(r\pi + d) \leq \alpha < \frac{2\pi}{l}(2r\pi + d) \\ f_4(\alpha \cdot \frac{l}{2\pi}) \ , & \frac{2\pi}{l}(2r\pi + d) \leq \alpha < 2\pi \end{cases} ,$$

where

$$\begin{aligned}
f_1(a) &= \begin{bmatrix} -r\sin(a/r) \\ -r\cos(a/r) \end{bmatrix} \ , \\
f_2(a) &= \begin{bmatrix} a - \pi r \\ r \end{bmatrix} \ , \\
f_3(a) &= \begin{bmatrix} -r\sin((a-d)/r) + d \\ -r\cos((a-d)/r) \end{bmatrix} \ , \\
f_4(a) &= \begin{bmatrix} l - a \\ -r \end{bmatrix} \ .
\end{aligned}$$

Lemma 1. *The inverse map* f^{-1} *is given by*

$$f^{-1}((x,y)^T) = \begin{cases} g_1(x,y) \cdot \frac{2\pi}{l} \ , & x < 0 \\ g_2(x,y) \cdot \frac{2\pi}{l} \ , & x \in [0,d] \wedge y > 0 \\ g_3(x,y) \cdot \frac{2\pi}{l} \ , & x > d \\ g_4(x,y) \cdot \frac{2\pi}{l} \ , & x \in [0,d] \wedge y \leq 0 \end{cases} ,$$

where

$$\begin{aligned}
g_1(x,y) &= r \cdot \left(\frac{3}{2}\pi - \mathrm{atan2}(y,x)\right) \ , \\
g_2(x,y) &= r \cdot \pi + x \ , \\
g_3(x,y) &= l - x \ , \\
g_4(x,y) &= d + r \cdot (2\pi - \mathrm{mod}(\mathrm{atan2}(y, x-d) + \pi/2, 2\pi)) \ .
\end{aligned}$$

Lemma 2. *The map* f *is a homeomorphism between manifolds.*

Proof. Obviously, S^1 and T are one-dimensional manifolds. It remains to show that f is a homeomorphism.

1) f is bijective: This follows from $f(S^1) = T$ together with $f^{-1} \circ f = id_{S^1}$.
2) f is continuous: Since f_1, f_2, f_3, f_4 are continuous, it is sufficient to check that

$$\begin{aligned}
f_1(0) &= f_4(2\pi) \\
f_2\left(\frac{2\pi}{l} r\pi\right) &= f_1\left(\frac{2\pi}{l} r\pi\right) \\
f_3\left(\frac{2\pi}{l}(r\pi + d)\right) &= f_2\left(\frac{2\pi}{l}(r\pi + d)\right) \\
f_4\left(\frac{2\pi}{l}(2r\pi + d)\right) &= f_3\left(\frac{2\pi}{l}(2r\pi + d)\right) \ .
\end{aligned}$$

   These four equations hold as can be shown by simply plugging in the values as given above.
3) f^{-1} is continuous: Similar to continuity of f. □

Lemma 3. *The homeomorphism* f *is length-ratio-preserving with* $c = \frac{||S^1||}{||T||} = \frac{2\pi}{l}$.

Proof. It is sufficient to show that $f_i(\alpha \cdot \frac{l}{2\pi})$ is length-ratio-preserving for $i = 1, 2, 3, 4$. We calculate

$$\begin{aligned}
\left|\left|\frac{\partial f_1(a)}{\partial a}\right|\right| &= \left|\left|\begin{bmatrix} -\cos(a/r) \\ +\sin(a/r) \end{bmatrix}\right|\right| \\
&= \sqrt{\cos^2(a/r) + \sin^2(a/r)} \\
&= 1 \ ,
\end{aligned}$$

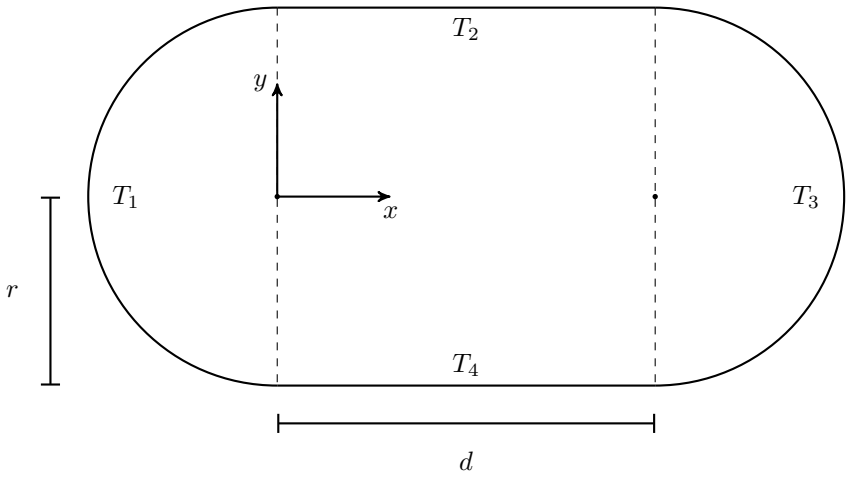

Fig. 3: The train track T we consider in this paper.

and similarly

$$\left|\left|\frac{\partial f_2(a)}{\partial a}\right|\right| = \left|\left|\frac{\partial f_3(a)}{\partial a}\right|\right| = \left|\left|\frac{\partial f_4(a)}{\partial a}\right|\right| = 1 \ .$$

For an injective smooth curve $\alpha : [0,1] \to T_i$ with $i \in \{1,2,3,4\}$, it follows that

$$\begin{aligned}
c \cdot ||f(\alpha)|| =& \frac{2\pi}{l} \cdot \int_0^1 \left|\left| \frac{\partial}{\partial t}\Big(f(\alpha(t))\Big) \right|\right| \, \mathrm{d}t \\
=& \frac{2\pi}{l} \cdot \int_0^1 \left|\left| \left(\frac{\partial}{\partial \alpha(t)} f(\alpha(t))\right) \frac{\partial}{\partial t}\alpha(t) \right|\right| \, \mathrm{d}t \\
=& \frac{2\pi}{l} \cdot \int_0^1 \left|\left| \frac{\partial}{\partial \alpha(t)} f(\alpha(t)) \right|\right| \cdot \left|\left| \frac{\partial}{\partial t}\alpha(t) \right|\right| \, \mathrm{d}t \\
=& \frac{2\pi}{l} \cdot \int_0^1 \left|\left| \frac{\partial}{\partial \alpha(t)} f_i\left(\alpha(t) \cdot \frac{l}{2\pi}\right) \right|\right| \\
& \cdot \left|\left| \frac{\partial}{\partial t}\alpha(t) \right|\right| \, \mathrm{d}t \\
=& \frac{2\pi}{l} \cdot \int_0^1 \left|\left| \frac{\partial}{\partial a} f_i(a) \cdot \frac{l}{2\pi} \right|\right| \cdot \left|\left| \frac{\partial}{\partial t}\alpha(t) \right|\right| \, \mathrm{d}t \\
=& \int_0^1 \underbrace{\left|\left| \frac{\partial}{\partial a} f_i(a) \right|\right|}_{1} \cdot \left|\left| \frac{\partial}{\partial t}\alpha(t) \right|\right| \, \mathrm{d}t \\
=& \int_0^1 \left|\left| \frac{\partial}{\partial t}\alpha(t) \right|\right| \, \mathrm{d}t \\
=& ||\alpha|| \ . \qquad \square
\end{aligned}$$

IV. Circular Filtering

We now present a filtering scheme based on circular probability distributions, which allows for recursive filtering on the circle S^1. The proposed filter is described in more detail in [5]. It draws inspiration from the similar circular filter published by [3] and from the unscented Kalman filter [16].

A. Circular Distributions

In order to derive the circular filter, we first introduce three circular probability distributions that will be used by the filter.

Definition 4. *(Wrapped normal distribution)*

A wrapped normal (WN) *distribution is given by the probability density function (pdf)*

$$f(x;\mu,\sigma) = \frac{1}{\sqrt{2\pi}\sigma} \sum_{k=-\infty}^{\infty} \exp\left(-\frac{(x-\mu+2k\pi)^2}{2\sigma}\right)$$

with parameters μ and $\sigma > 0$.

The WN distribution is a natural distribution to use on the circle because it fulfills the central limit theorem. It is closed under convolution, but not under multiplication of pdfs.

Definition 5. *(Von Mises distribution)*

A von Mises (VM) *distribution is given by the pdf*

$$f(x;\mu,\kappa) = \frac{1}{2\pi I_0(\kappa)} \exp(\kappa \cos(x-\mu))$$

with parameters μ and $\kappa > 0$ where I_0 is the modified Bessel function of order 0.

The VM distribution is also commonly used on the circle because it is easier to use than a wrapped normal distribution as it avoids the infinite series. It is closed under multiplication of pdfs, but not under convolution.

Definition 6. *(Wrapped Dirac mixture distribution)*

A wrapped Dirac mixture (WD) *distribution with $L \in \mathbb{N}$ components is given by*

$$f(x;\beta_1,\ldots,\beta_L,w_1,\ldots,w_L) = \sum_{k=1}^{L} w_k \delta(x-\beta_k)$$

with Dirac positions $\beta_1,\ldots,\beta_L$ and weights $w_1,\ldots,w_L$. Each component is a weighted Dirac δ distribution.

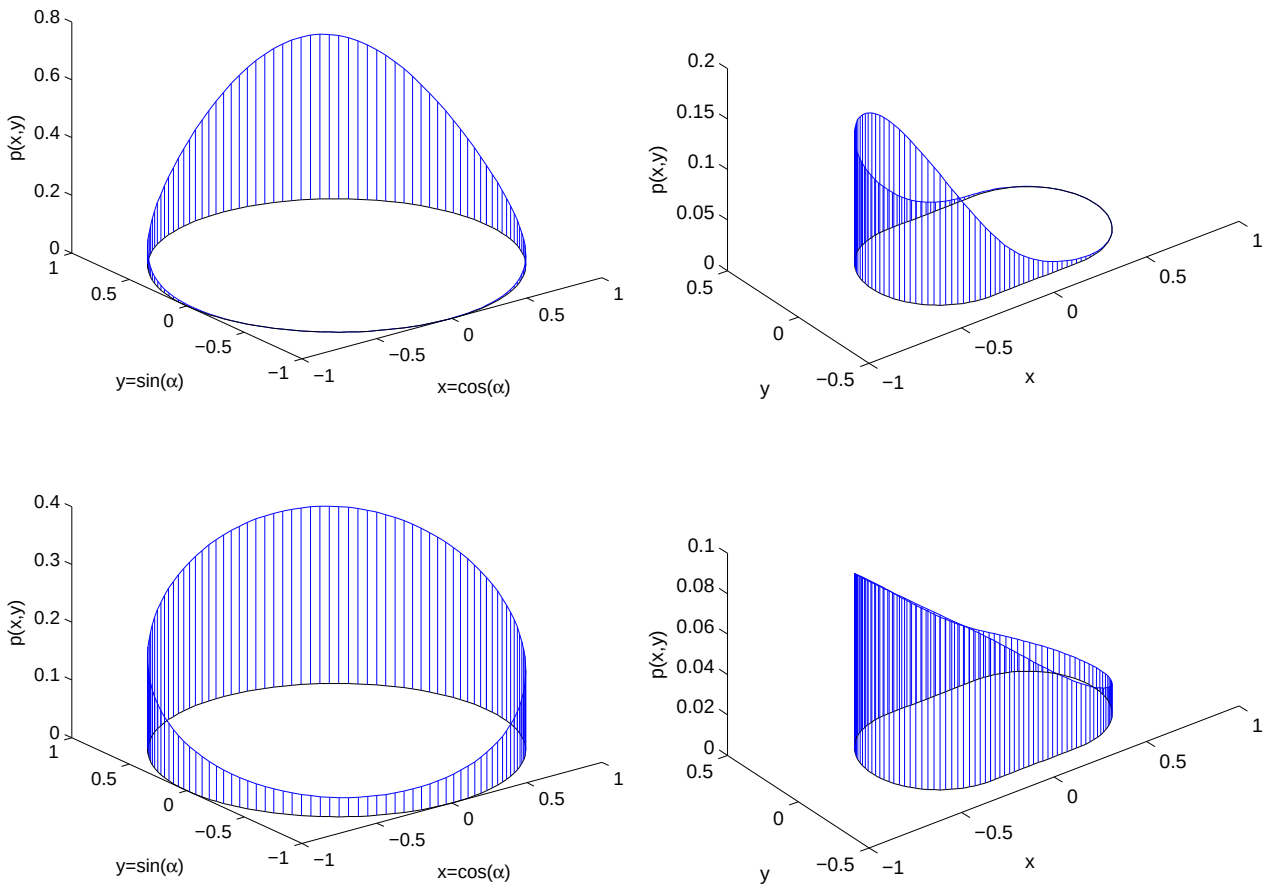

Fig. 4: Wrapped normal probability density function on the circle S^1 (left) and probability density function on the manifold T (right) for two $\sigma = 0.7\,\text{rad}$ (top) and $\sigma = 1.3\,\text{rad}$ (bottom).

B. Circular Moment Matching

Definition 7. *(Circular moment)*

The n-th circular moment of a random variable X on the circle is given by

$$m_n = \mathbf{E}(\exp(inX)) = \int_0^{2\pi} \exp(inx) f(x)\,\mathrm{d}x \ ,$$

where i is the imaginary unit.

Thus, $m_n \in \mathbb{C}$ is a two-dimensional quantity. The first circular moment m_1 includes information about both mean and concentration of the random variable and can be seen as an analogue to the first two conventional moments.

Lemma 4. 1) *The n-th circular moment of a WN-distributed random variable with parameters μ and σ is given by*

$$m_n = \exp(in\mu - n^2\sigma^2/2) \ .$$

2) *The n-th circular moment of a VM-distributed random variable with parameters μ and κ is given by*

$$m_n = \exp(in\mu) I_n(\kappa)/I_0(\kappa) \ .$$

3) *The n-th circular moment of a WD-distributed random variable with parameters $\beta_1, \ldots, \beta_L$ and $w_1, \ldots, w_L$ is given by*

$$m_n = \sum_{k=1}^{L} \omega_k \exp(in\beta_k) \ .$$

Proof. The proof for 1) is given in [1] and the proofs for 2) and 3) are given in [2]. □

A numerically stable algorithm to calculate the ratio of Bessel functions occurring in the moments of the von Mises distribution can be found in [17]. Pseudo code for this algorithm is provided in [5].

Now, we can apply circular moment matching to approximate circular distributions of these types by one another. Detailed derivations for the approximations based on circular moment matching are given in [5].

Converting between the different probability distributions on the circle allows us to take advantage of their respective benefits for different steps during the filtering process. Noise is modeled as WN because it fulfills the central limit theorem. The WD distribution is used when a (possibly nonlinear) system

function has to be applied. Multiplication is performed with VM distributions and convolution is once again based on WN distributions.

C. Prediction

The algorithm for prediction is given in Algorithm 1. It is reminiscent of the UKF and essentially consists of the following steps. First, the prior WN distribution is converted to a WD distribution with three Dirac components. These are passed through the system function and the resulting WD distribution is converted back to a WN distribution. Subsequently, the convolution of this WN distribution with the system noise is calculated.

Input: a_k (system function),
μ_k^e, σ_k^e (estimated distribution of state),
μ_{w_k}, σ_{w_k} (distribution of system noise)

Output: μ_k^p, σ_k^p (predicted distribution of state)

/* Dirac approximation */
$\alpha \leftarrow \arccos\left(\frac{3}{2}\exp\left(-\frac{(\sigma_k^e)^2}{2}\right) - \frac{1}{2}\right)$;
/* application of system function */
$\beta_1 \leftarrow a_k(\mu_k^e - \alpha)$;
$\beta_2 \leftarrow a_k(\mu_k^e)$;
$\beta_3 \leftarrow a_k(\mu_k^e + \alpha)$;
/* conversion of Diracs back to WN */
$\mu \leftarrow \operatorname{atan2}\left(\sum_{j=1}^3 \sin(\beta_j), \sum_{j=1}^3 \cos(\beta_j)\right)$;
$\sigma \leftarrow \sqrt{-2\log\left(\frac{1}{3}\sum_{j=1}^3 \cos(\beta_j - \mu)\right)}$;
/* convolution with noise */
$\mu_k^p \leftarrow (\mu + \mu_{w_k}) \mod 2\pi$;
$\sigma_k^p \leftarrow \sqrt{\sigma^2 + \sigma_{w_k}^2}$;

Algorithm 1: Algorithm for prediction.

D. Update

The measurement update algorithm is given in Algorithm 2. The idea behind the algorithm is to use a Bayesian update step, which is achieved by multiplying the predicted pdf and the likelihood pdf. The likelihood can be obtained by shifting the measurement noise distribution accordingly. To carry out the multiplication, both WN distributions are converted to VM distributions and then multiplied. Finally, the result is converted back to a WN distribution.

V. Experiments

To evaluate the proposed algorithm, we conducted a tracking experiment and compared the result to two standard approaches. More specifically, we track a toy train that moves along the periodic track and is observed by a Microsoft Kinect from bird's eye view. Fig. 1 illustrates this scenario. The straight segments of the track both have a length of $d = 0.48\,\mathrm{m}$ and the two half circles both have a radius of $r = 0.36\,\mathrm{m}$. An illustration of these parameters is given in Fig. 3. Note that

Input: measurement $\hat{z}_k$,
μ_k^p, σ_k^p (predicted distribution of state),
μ_{v_k}, σ_{v_k} (distribution of measurement noise)

Output: μ_k^e, σ_k^e (estimated distribution of state)

/* shift f^v by measurement */
$\tilde{\mu}_{v_k} \leftarrow (\hat{z}_k - \mu_{v_k}) \mod 2\pi$;
$\tilde{\sigma}_{v_k} \leftarrow \sigma_{v_k}$;
/* convert to VM distribution */
$\mu_1, \kappa_1 \leftarrow$wnToVonMises$(\mu_k^p, \sigma_k^p)$;
$\mu_2, \kappa_2 \leftarrow$wnToVonMises$(\tilde{\mu}_{v_k}, \tilde{\sigma}_{v_k})$;
/* multiply densities */
$C \leftarrow \kappa_1 \cos\mu_1 + \kappa_2 \cos\mu_2$;
$S \leftarrow \kappa_1 \sin\mu_1 + \kappa_2 \sin\mu_2$;
$\mu \leftarrow \operatorname{atan2}(S, C)$;
$\kappa \leftarrow \sqrt{S^2 + C^2}$;
/* convert back to WN distribution */
$\mu_k^e, \sigma_k^e \leftarrow$vonMisesToWn$(\mu, \kappa)$;

Algorithm 2: Algorithm for measurement update.

the entire scenario lies within the field of view of the Kinect as can be seen in Fig. 5.

A chessboard was carefully aligned with the track in order to determine its relative pose to the sensor (see Fig. 1). Due to the even ground plane, the train could easily be extracted from the depth images by clipping. In doing so, points that originate exclusively from the top side of the train could be obtained. The ground truth for the position of the train at each frame was calculated as the mean of all extracted points.

For the tracking task, one of the measured points was selected randomly and provided to the competing estimators, i.e., the proposed approach and two standard methods. Selecting single points instead of the entire point cloud allows for simulating a sensor that is affected by a large uncertainty.

As standard approaches we considered

1) the 1D Kalman filter from Sec. II-A that directly estimates the angle and ignores all circular singularities, and
2) the 2D Kalman filter from Sec. II-B that estimates a full two-dimensional position and projects the posterior position back onto the track.

The behavior of the train was modeled as approximately constant velocity for all estimators and the noise parameters were obtained from the ground truth by calculating the empirical mean and covariance. The parameters of the system noise for the 2D KF are

$$\mu_{\text{sys}}^{2D} = \begin{bmatrix} -3.091 \cdot 10^{-4} \\ +3.854 \cdot 10^{-7} \end{bmatrix}$$

and

$$C_{\text{sys}}^{2D} = \begin{bmatrix} +2.353 \cdot 10^{-5} & -3.304 \cdot 10^{-7} \\ -3.304 \cdot 10^{-7} & +1.064 \cdot 10^{-5} \end{bmatrix},$$

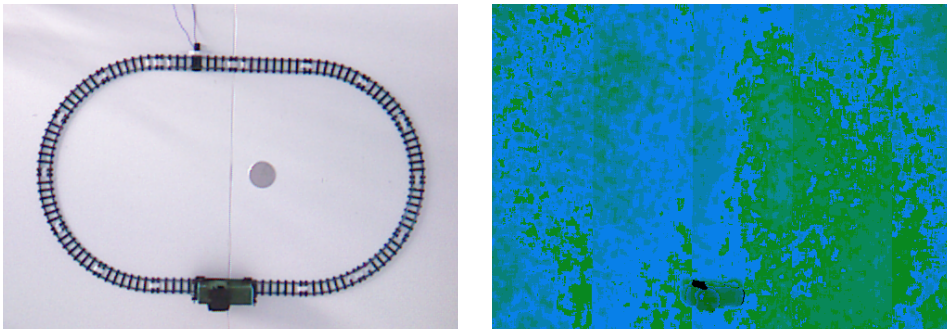

Fig. 5: Color and depth images of the scene as obtained by the Kinect.

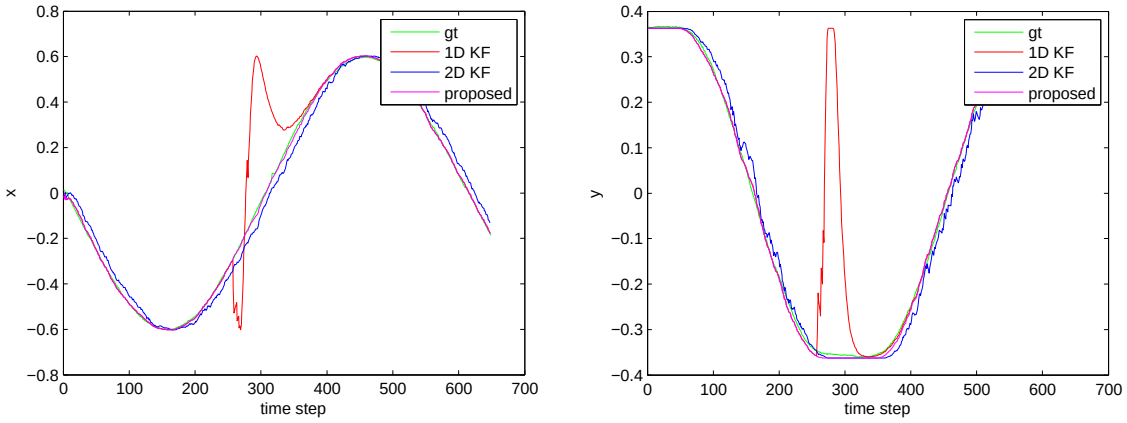

Fig. 6: True and estimated trajectories in x- and y-direction for one lap.

where the units are m and m^2 respectively. The measurement noise is zero-mean and has covariance

$$C^{2D}_{\text{meas}} = \begin{bmatrix} 2.558 \cdot 10^{-3} & 2.495 \cdot 10^{-5} \\ 2.495 \cdot 10^{-5} & 3.150 \cdot 10^{-4} \end{bmatrix}$$

measured in m^2.

For the 1D KF and the proposed approach, we used the system noise parameters

$$\mu^{1D}_{\text{sys}} = 6.273 \ , \quad \sigma^{1D}_{\text{sys}} = 4.684 \cdot 10^{-3} \ ,$$

and zero-mean measurement noise with

$$\sigma^{1D}_{\text{meas}} = 9.813 \cdot 10^{-2} \ ,$$

where all units are radians.

The results for one representative lap are depicted in Fig. 6 and Fig. 8. Note that time is drawn on the z-axis. An analysis of the estimation error compared to the ground truth is shown in Fig. 7. As can be seen on the plots, the proposed estimator performs well across the entire run. The 2D KF produces inferior results throughout the experiment and the 1D KF performs well at first, but fails completely once the discontinuity in the transformation is reached.

VI. Conclusion

In this paper, we have presented an approach to constrained target tracking based on performing a topological transformation to a circle and applying a circular filtering algorithm.

We have shown the viability of the proposed method in real experiments by tracking the movement of a toy train on a two-dimensional track. A comparison with traditional approaches based on Kalman filters shows the clear superiority of the method based on directional statistics.

Future work may include the generalization of the proposed approach to two-dimensional manifolds, which can be mapped to simple shapes like a sphere or a torus depending on their topology. A filtering scheme based on probability distributions on the sphere or torus could then be used to track an object whose movement is constrained to the considered two-dimensional manifold.

Acknowledgment

This work was partially supported by the German Research Foundation (DFG) within the Research Training Group RTG 1126 "*Intelligent Surgery - Development of new computer-based methods for the future working environment in visceral surgery*".

References

[1] K. V. Mardia and P. E. Jupp, *Directional Statistics*, 1st ed. Wiley, 1999.
[2] S. R. Jammalamadaka and A. Sengupta, *Topics in Circular Statistics*. World Scientific Pub Co Inc, 2001.
[3] M. Azmani, S. Reboul, J.-B. Choquel, and M. Benjelloun, "A recursive fusion filter for angular data," in *IEEE International Conference on Robotics and Biomimetics (ROBIO)*, 2009, pp. 882–887.

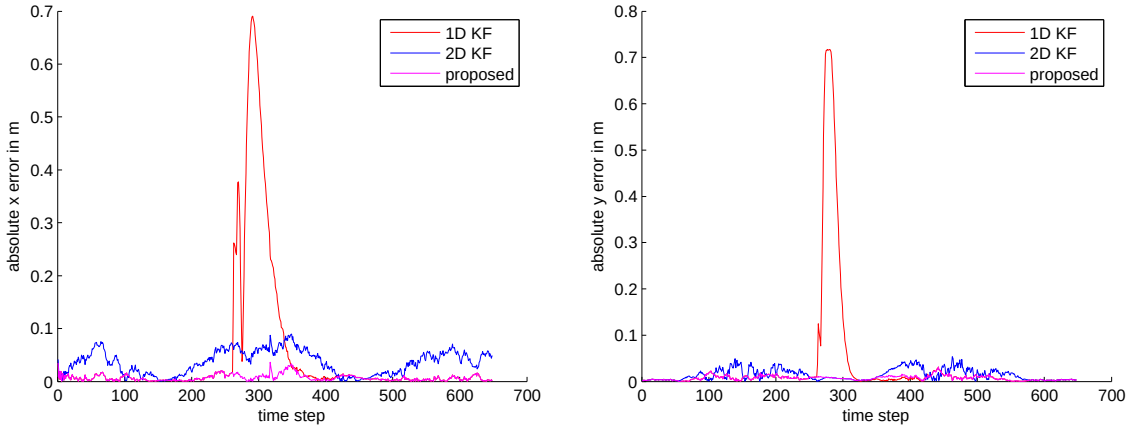

Fig. 7: Absolute error in x- and y-direction across one lap.

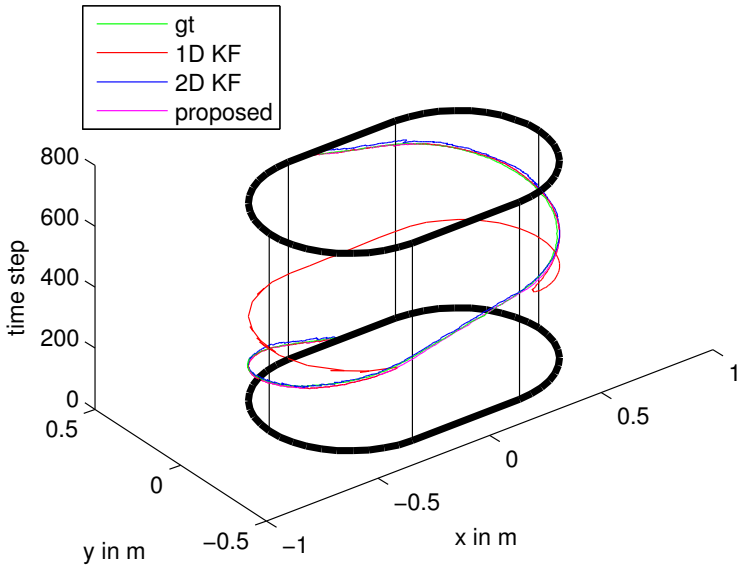

Fig. 8: True and estimated trajectories for one lap.

[4] G. Stienne, S. Reboul, M. Azmani, J. Choquel, and M. Benjelloun, "A multi-temporal multi-sensor circular fusion filter," *Information Fusion*, 2013.

[5] G. Kurz, I. Gilitschenski, and U. D. Hanebeck, "Recursive Nonlinear Filtering for Angular Data Based on Circular Distributions," in *Proceedings of the 2013 American Control Conference (ACC 2013)*, Washington D. C., USA, Jun. 2013.

[6] W. Feiten, P. Atwal, R. Eidenberger, and T. Grundmann, "6d pose uncertainty in robotic perception," in *Advances in Robotics Research*. Springer Berlin Heidelberg, 2009, pp. 89–98.

[7] W. Feiten, M. Lang, and S. Hirche, "Rigid motion estimation using mixtures of projected gaussians," in *Proceedings of the 16th International Conference on Information Fusion (Fusion 2013)*, 2013.

[8] G. Kurz, I. Gilitschenski, S. J. Julier, and U. D. Hanebeck, "Recursive Estimation of Orientation Based on the Bingham Distribution," in *Proceedings of the 16th International Conference on Information Fusion (Fusion 2013)*, Istanbul, Turkey, Jul. 2013.

[9] D. Simon, "Kalman filtering with state constraints: a survey of linear and nonlinear algorithms," *IET Control Theory & Applications*, vol. 4, no. 8, pp. 1303–1318, 2010.

[10] C. Yang, M. Bakich, and E. Blasch, "Nonlinear constrained tracking of targets on roads," in *7th International Conference on Information Fusion (FUSION)*, Philadelphia, Pennsylvania, 2005.

[11] L.-S. Wang, Y.-T. Chiang, and F.-R. Chang, "Filtering method for nonlinear systems with constraints," *IEE Proceedings - Control Theory and Applications*, vol. 149, no. 6, p. 525, 2002.

[12] C. Yang and E. Blasch, "Kalman filtering with nonlinear state constraints," *Aerospace and Electronic Systems, IEEE Transactions on*, vol. 45, no. 1, pp. 70–84, 2009.

[13] S. Julier and J. LaViola, "On Kalman filtering with nonlinear equality constraints," *IEEE Transactions on Signal Processing*, vol. 55, no. 6, pp. 2774–2784, 2007.

[14] T. Gindele, S. Brechtel, J. Schroder, and R. Dillmann, "Bayesian Occupancy grid Filter for dynamic environments using prior map knowledge," in *2009 IEEE Intelligent Vehicles Symposium*. Ieee, Jun. 2009, pp. 669–676.

[15] R. E. Kalman, "A New Approach to Linear Filtering and Prediction Problems," *Transactions of the ASME Journal of Basic Engineering*, vol. 82, pp. 35–45, 1960.

[16] S. J. Julier and J. K. Uhlmann, "Unscented filtering and nonlinear estimation," *Proceedings of the IEEE*, vol. 92, no. 3, pp. 401–422, Mar. 2004.

[17] D. E. Amos, "Computation of modified Bessel functions and their ratios," *Mathematics of Computation*, vol. 28, no. 125, pp. 239–251, 1974.